

Reactions of abiogenic hydrocarbons in Earth's upper mantle

Nore Stolte,^{1,*} Tao Li,^{1,†} and Ding Pan^{1,2,‡}

¹*Department of Physics, Hong Kong University of Science and Technology, Hong Kong, China*

²*Department of Chemistry, Hong Kong University of Science and Technology, Hong Kong, China*

(Dated: June 17, 2025)

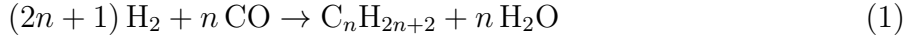
Abstract

The formation of hydrocarbon fuels in Earth's interior has traditionally been considered to have biogenic origins; however, growing evidence suggests that some light hydrocarbons may instead originate abiotically. It is widely expected that the Fisher-Tropsch-type (FTT) process, which typically refers to the conversion of inorganic carbon to organic matter in the geologic convention, may also happen in Earth's interior, but the aqueous conditions and absence of industrial catalysts in deep environments suggest that the FTT process can be very different from that in the chemical industry. Here, we performed extensive ab initio molecular dynamics (AIMD) simulations (> 2.4 ns) to investigate the FTT synthesis in dry mixture and in aqueous solutions at 10-13 GPa and 1000-1400 K. We found that large hydrocarbon-related species containing C, O, and H are abiotically synthesized via the polymerization of CO without any catalyst. Supercritical water, commonly found in deep Earth, does not prevent organic molecule formation but restricts product size and carbon reduction. Our studies reveal a previously unrecognized abiogenic route for hydrocarbon synthesis in mantle geofluids. These carbon-containing fluids could potentially migrate from depth to shallower crustal reservoirs, thereby contributing to the deep carbon cycle, influencing surface carbon budgets, and possibly serving as a new energy source.

INTRODUCTION

Abiogenic hydrocarbons have been identified in diverse terrestrial environments, including the Canadian Kidd Creek Mine [1], South Africa’s Witwatersrand Basin [2], the Lost City Hydrothermal Field in the Atlantic Ocean [3], and the Junggar Basin in northwestern China [4]. Their formation from abiogenic precursors in Earth’s interior influences carbon distribution in the deep carbon cycle [5, 6], with substantial effects on surface and atmospheric carbon reservoirs. Furthermore, abiogenic hydrocarbons generated in the crust and mantle contribute to natural gas and petroleum deposits, potentially affecting fossil fuel availability [6, 7]. The origins of abiogenic hydrocarbons have been debated in the scientific literature for decades (e.g., [8–11]). However, their formation mechanisms remain largely unknown.

The Fisher-Tropsch (FT) process is an important synthesis method to produce liquid hydrocarbons in chemical engineering [12]. It includes a series of catalytic reactions converting CO and H₂ into heavier hydrocarbons as:



Many geochemists anticipate that such reactions may also occur in deep Earth to generate abiogenic hydrocarbons in a reducing environment, though industrial catalysts such as transition metal alloys typically do not exist in natural environments. In the relevant studies, the Fischer-Tropsch-type (FTT) synthesis typically refers to the conversion of inorganic carbon to organic matter in a broader context [13]. The FTT synthesis in natural environments is typically evidenced by the distribution of ¹³C and ¹²C across hydrocarbons in the sample [1, 3]. Another key difference between industrial and geochemical FTT synthesis is the presence of water. Despite the production of a small amount of water, industrial FTT reactions typically occur in dry gas mixtures without any liquid water, whereas in subsurface geologic environments, the FTT process occurs in the medium of liquid or supercritical water [13]. The influence of the aqueous environment on the FTT process is poorly understood.

In Earth’s upper mantle, at depths of 100–420 km, pressure (P) and temperature (T) reach approximately 13 GPa and 1700 K, respectively [14]. Experimental investigation of chemical reactions under such extreme P-T conditions remains highly challenging [15]. First-principles atomistic simulations, which require neither experimental input nor empirical parameters, have been successfully applied to study prebiotic chemistry, providing crucial molecular-level insights [16]. Spanu et al. applied ab initio molecular dynamics (AIMD) simulations to show that larger hydrocarbons are thermodynamically favored in Earth’s deep interior [17]. However, the reaction pathways for methane conversion to higher hydrocarbons still require clarification. Kuang and Tse applied AIMD to study reactions between H_2 and $CaCO_3$ under extreme P-T conditions corresponding to Earth’s lower mantle and core-mantle boundary, observing the formation of tetrahedral C_4 moieties and water [18]. Additional studies have explored methane reactions and stability at megabar pressures and temperatures of several thousand kelvins—conditions more extreme than Earth’s mantle and typical of ice giant planets like Neptune and Uranus [19–21]. Nevertheless, our understanding of abiogenic hydrocarbon reactions under upper mantle conditions remains very limited.

In this work, we studied the abiogenic synthesis of hydrocarbons at 10–13 GPa and 1000–1400 K found in Earth’s upper mantle. We conducted extensive ab initio molecular dynamics (AIMD) simulations, with a cumulative duration exceeding 2.4 ns, to investigate the uncatalyzed reactions of the FTT reactants $CO + H_2$ in a dry mixture and in aqueous solutions. We found that large hydrocarbon-related species containing C, O, and H are abiotically synthesized via the polymerization of CO both in aqueous and dry mixtures, and that reactions of polymers with H_2 lead to reduction of carbon. Higher pressure leads to formation of more organic species and larger products. Water does not prevent organic molecule formation but restricts product size and carbon reduction. Finally, we discussed reaction mechanisms of abiogenic organic synthesis and implications to new source of hydrocarbon fuels in Earth’s upper mantle.

RESULTS

We first carried out AIMD simulations of a 1:1 supercritical mixture of CO and H₂ at 13 GPa and 1400 K. Then, we added water to the mixture, and performed AIMD simulations of 1:1:1 supercritical mixtures of CO, H₂, and H₂O at 10–13 GPa and 1000–1400 K (Table SI in the supporting information). At each condition, we performed six independent 50 ps long (after equilibration) NVT simulations, giving a total of 300 ps of simulation at equilibrium for each condition. We analyzed the whole trajectories to uncover reaction mechanisms.

In all systems studied, the C-C and C-H radial distribution functions (RDFs) show a pronounced peak at covalent-bonding distances (Fig. 1), even though initially, there were only CO, H₂ and H₂O molecules in the supercritical mixtures. The C-C RDFs have a maximum at 1.40–1.47 Å, indicating that there is likely a mixture of C-C single bonds (bond length ~1.54 Å) and C=C double bonds (bond length ~1.34 Å) present in the fluids. The C-H RDFs have the first maximum at 1.09 Å. The C-H bond length in alkanes or alkenes is ~1.09 Å, so we can conclude that C-H covalent bonds form in the supercritical mixtures. Also, the C-C RDFs show enhanced structuring beyond the first peak, in particular at 13 GPa and 1400 K, indicating that extended molecules are present.

The overview of reaction products in Fig. 2 indeed shows that larger products form at larger pressure, and that products are larger in the absence of water. At equilibrium in the dry CO + H₂ mixture at 13 GPa and 1400 K, more than half the CO molecules had reacted to form molecules containing three or more C atoms, and 43 % of all carbon was contained in molecules with 7 or more C atoms (Fig. 3). Typically, product molecules of the reactions between CO and H₂ at these conditions contain carbonyl bonds, ether bonds, hydroxyl bonds, C-H bonds, and rings incorporating both oxygen and carbon atoms. Some minor C₁ products formed as well, namely carbon dioxide and formaldehyde, but CO molecules still make up the majority of C₁ molecules.

After adding water to the supercritical mixture of CO and H₂ at 13 GPa and 1400 K,

polymerization of carbon still took place, but at equilibrium the carbon-containing molecules are smaller than in the dry mixture. C_1 molecules make up 61 % of the total C content at 13 GPa and 1400 K in the $CO + H_2 + H_2O$ mixture (Fig. 3). Carbon monoxide remains the most important C_1 molecule, with some CO_2 , $HCOOH$ and $HCOO^-$ species forming as well. About 5 % of the carbon is contained in molecules with more than 6 C atoms, and C_4 , C_5 and C_6 molecules are more abundant in the aqueous mixture than in the dry one. This indicates that water does not inhibit polymerization of CO at extreme conditions, but it does affect the size of the reaction products.

When we decreased the pressure to 10 GPa at 1400 K for the $CO + H_2 + H_2O$ mixture, carbon-containing molecules decreased in size, and no molecules larger than C_5 were formed (Fig. 3). Additionally, at 10 GPa the first peak in the C-H RDF is significantly smaller than at 13 GPa, i.e., decreasing pressure leads to formation of fewer C-H bonds (Fig. S5). The effect of pressure can be understood through the reaction stoichiometry. In polymerization reactions, several small reactant molecules react to form one large product molecule, so the effective volume of the reaction product is smaller than that of the reactants. The Gibb's free energy change of reaction is given by $\Delta U + P\Delta V - T\Delta S$, where U is the internal energy, V is the volume, and S is the entropy. For polymerization reactions, $P\Delta V$ is negative, and it is more negative at larger pressure. Therefore, product molecules are smaller and C_1 molecules are more abundant at 10 GPa than at 13 GPa at the same temperature.

Finally, we decreased the temperature from 1400 K to 1000 K at 10 GPa for $CO + H_2 + H_2O$. With decreasing temperature, the first peak in the C-C RDF increased in height, meaning that more C-C bonds form at lower temperatures. At 1000 K, C_1 molecules make up a smaller fraction of the total carbon content than at 1400 K, and more C_5 molecules exist at lower temperature (Fig. 3). Overall, larger molecules form at 1000 K than at 1400 K at the same pressure because of entropic effects. Less entropy is associated with large molecules than with small ones, so for polymerization reactions, $T\Delta S$ is negative, i.e., there is a free energy penalty associated with formation of large molecules. The free energy penalty

increases with temperature, so larger molecules are more stable at lower temperature.

In the solutions studied here, reactions that led to polymerization of carbon were initiated when a C-C bond formed between CO molecules. A chain of CO molecules bonded through the carbon atoms is thermodynamically unstable relative to separated CO molecules [22–24], and in our simulations such chains tended to react further within a few picoseconds. In some cases, H₂ dissociated to form C-H bonds with carbon atoms and C-OH bonds with oxygen atoms in the CO polymers, which stabilized molecules as bonds became saturated. If a polymer was not stabilized by termination with H₂, it tended to react with further CO molecules, which increased the size of the molecule, as shown in Fig. S6.

Alternatively, molecules reached stable configurations by forming a ring, as can be seen in Fig. 2. At equilibrium, these rings have 4 to 8 vertices, and typically incorporate at least one oxygen atom, such as substituted oxetane, (di)oxolane, and (di)oxane rings. We did not find any three-membered rings, which have quite a strained geometry. The most extreme case of stabilization of a polymer through the formation of a ring that we observed in our simulations was the formation of neutral cyclobutane-1,2,3,4-tetrone (C₄O₄) from 4 CO molecules in the CO + H₂ mixture at 13 GPa and 1400 K (Fig. S7 in the supporting information). In the gas phase, C₄O₄ is thermodynamically unstable relative to 4 CO molecules [25], though it has been studied using negative ion photoelectron spectroscopy [26]. In supercritical mixture of CO and H₂, C₄O₄ in one case had a lifetime exceeding 20 ps, so it is possible that the high pressure leads to stabilization of the triplet state molecule.

When water was present, the molecules could be stabilized in a further way as well. In addition to reactions with H₂ and formation of rings, (CO)_n polymers were stabilized through reactions with H₂O. H₂O can donate H⁺ or OH[−], or both, to the polymer, forming C-H and C-OH bonds. Unstable CO chains readily react with further CO molecules, thereby increasing the size of the molecule, but molecules that are saturated by C-H or C-OH bonds are not so reactive. Therefore, water affects the carbon polymerization reactions in CO + H₂ + H₂O solutions by saturating bonds in the unstable CO chains, which prevents further CO

molecules from bonding to the polymer, resulting in smaller reaction products. The stable end groups on the carbon polymers formed by reactions with water or H₂ also prevent rings from forming in the molecule, so cyclic compounds are less abundant in the presence of water (Fig. 2). A CO polymerization reaction mechanism with water is illustrated in Fig. 4. Initially, three CO molecules bond through their carbon atoms. Water dissociates to form a new hydroxyl group at a terminal carbon atom, while donating the second hydrogen atom to the central CO unit, forming another hydroxyl group. The carbon atom at the other end reacts with CO, which increases the size of the molecule to C₄. At this end, a H₂ atom dissociates, and one of its atoms forms a C-H bond. The second atom is donated to an oxygen atom of the same molecule with the participation of a water molecule. This leaves 2,3-hydroxy-4-oxobut-2-enoic acid. A CO polymerization reaction in the dry CO + H₂ mixture is illustrated in Fig. S7 in the supporting information.

One final way in which CO polymers reached a stable configuration was through the breaking of the carbon monoxide C-O bonds. Although this happened rarely in our simulations, we observed a few instances where three CO molecules bonded through the carbon atoms, and the central C-O bond broke to leave a stable linear carbon suboxide molecule, C₃O₂ (Fig. S8 in the supporting information). In the industrial FT synthesis, the breaking of the C-O bond of carbon monoxide at the catalyst surface is a central step in the reaction pathway, so the fact that C-O bonds broke so rarely in reactions studied here illustrates that the reaction mechanisms that we observed are distinct from those involved in the industrial FT synthesis.

Another remarkable observation is that no C₂ molecules formed during our NVT simulations (Fig. 3), both with and without water. The dimer of CO (ethylene dione) is energetically unstable with respect to dissociation to two CO molecules even though its ground state is a triplet state, as the singlet-triplet crossing point occurs close to the triplet energy minimum with respect to the bend angle [22, 24]. As a result, any CO molecules that do temporarily form a covalent OC-CO bond, as defined by the C-C distance, rapidly

dissociate again, before the molecule can be stabilized in further reactions.

The oxidation state of carbon in CO is +2, but formation of new C-O and C-H bonds alters the carbon oxidation state. In the dry CO + H₂ mixture at 13 GPa and 1400 K, the average oxidation state of carbon in the system was reduced to +1.79 ± 0.08 at 13 GPa, 1400 K (Fig. 5). The main cause of this reduction is the formation of C-H bonds, rather than the breaking of C-O bonds. As discussed, we rarely observed breaking of the C-O bond, and when a C-O bond was broken, it always led to the formation of CO₂, where carbon has an oxidation state of +4. In the presence of water, the average oxidation state of carbon is +1.89 ± 0.06 at 13 GPa and 1400 K. In aqueous solutions, not only did C-O bonds break, but new C-O bonds formed as well, because H₂O reacted with CO molecules, forming CO₂, HCOOH, and oxygen-rich polymers. Therefore, carbon is more oxidized when water is present in the reaction mixture, though carbon is still reduced relative to its oxidation state in CO. The average oxidation state of carbon atoms is only slightly below +2 for the CO + H₂ + H₂O mixture at 10 GPa and 1400 K. This slight reduction of carbon is due to the formation of C-H bonds, which occurs less readily at 10 GPa than at 13 GPa (Fig. S5 in the supporting information). The oxidation state of carbon does not change when going from 1400 K to 1000 K at 10 GPa, because the number of new C-O and C-H bonds that forms at both conditions is nearly equal (Fig. S5 in the supporting information). Overall, we find that at the conditions studied, temperature does not substantially affect the oxidation state of carbon, but increasing pressure leads to the reduction of carbon, primarily as a result of the formation of C-H bonds. In the presence of water, the formation of new C-O bonds results in more oxidized carbon products than in the dry CO + H₂ mixture at the same P-T conditions.

DISCUSSION

Abiogenic synthesis of hydrocarbons from supercritical C-O-H fluids could take place under Earth's upper mantle conditions, even without any catalyst. The carbon polymerization reaction mechanism in our study is distinctly different from the FTT synthesis that occurs in hydrothermal environments[13, 27–29], because the extreme pressure plays an important role. Higher pressures lead to increased stabilization of large molecules for addition reactions, and more organic species and larger size of hydrocarbons ($>\text{C}_6$) are formed at 13 GPa. During the synthesis process, carbon in CO does not need to be reduced before a polymer forms, and in fact, H₂ molecules dissociate and react with the polymer of CO molecules only *after* the reaction is initialized through formation of C-C bonds. More importantly for Earth's upper mantle environment, we find that water does not inhibit C-C bond formation, as evidenced by the generation of molecules containing up to five C-C bonds in our simulations. However, carbon does remain more oxidized in aqueous solutions than in dry mixtures of CO and H₂ because reactions with water lead to formation of new C-O bonds, and these hydrocarbon-related products have larger oxygen content. Higher pressure is conducive to the reduction of carbon due to the formation of C-H bonds. These organic species are notably characterized by a significant presence of oxygen atoms. However, it's important to emphasize that these compounds do not necessarily represent the final products formed in real geofluid environments. In our study, due to the limited size of the systems in AIMD simulations, we focused primarily on the internal reactions of C-H-O fluids. The environment of Earth's interior is considerably more complex, containing a diverse array of metallic elements such as Fe, Ca, Mo, Ni, and Cr which were not included in this simulation. These elements have the potential to act as deoxidizers, catalyzing the reduction of oxygen-containing compounds into hydrocarbons [30–36].

Our results reveal another possible route of abiogenic synthesis of higher hydrocarbon-related species in geofluids in Earth's upper mantle. In fact, mantle-derived hydrocarbons

have been found in hydrothermal fields [37, 38], providing evidence that hydrocarbons indeed form at the extreme conditions of the mantle. We show that carbon in the form of CO can polymerize in regions of the mantle where water is abundant, such as in subduction zones. Subduction zones are important regions in the deep carbon cycle, as downgoing tectonic plates carry vast amounts of carbon from Earth’s surface to its interior, and the amount of carbon that is released from the plate in the crust and upper mantle to a large extent determines the carbon budget at Earth’s surface [5, 39]. Organic products may play a role in the deep carbon cycle, as carbon-containing fluids are transported from depth to Earth’s crust [40]. More importantly, abiotically synthesized hydrocarbons as suggested by our study may also have the chance to migrate to the shallower regions of the Earth through deep faults or plate boundaries in some weak subduction zones [15], contributing to oil and gas reservoirs [41].

CONCLUSION

In summary, we studied the FTT synthesis under aqueous conditions without catalysts. our extensive AIMD simulations (>2.4 ns) show that hydrocarbons and related organic species can be abiotically synthesized under upper mantle conditions (10–13 GPa, 1000–1400 K) through CO polymerization, even in the absence of catalysts. Different from FTT reactions in industrial environments, extreme pressure promotes C–C bond formation and stabilizes larger hydrocarbons($>C_6$). Supercritical water is common in Earth’s deep interior. While it does not inhibit organic synthesis, it limits product size and carbon reduction compared to dry CO-H₂ mixtures. Our study highlights a previously unrecognized route for abiotic hydrocarbon synthesis in Earth’s deep interior, with implications for the deep carbon cycle and potential energy resources. Future work would be expected to explore the role of minerals in deep Earth to better understand abiogenic formation process of hydrocarbons.

METHODS

Ab initio molecular dynamics (AIMD) simulations

We carried out Born-Oppenheimer AIMD simulations using the Qbox code [42]. Here, we have used the PBE exchange-correlation functional [43]. Previously, we found that the discrepancies between results obtained with the PBE and the hybrid PBE0 functional [44] are significantly smaller at extreme P-T conditions than at ambient conditions [45–47]. For example, the PBE and PBE0 results for speciation of $\text{CO}_2(\text{aq})$ at upper mantle conditions are qualitatively equivalent [47]. Because the PBE and PBE0 functionals do not adequately describe van der Waals (vdW) interactions, we additionally tested vdW corrections using Grimme’s D3 method [48] with Becke-Johnson damping implemented in the RPBE-D3 functional [49]. We found these corrections produced only minor variations (<6%) in carbon species mole fractions [50]. This confirms that dispersion interactions play an insignificant role in covalent bond transformations and consequently have negligible effects on the observed chemical speciation. Therefore, we expect that our results for the carbon speciation at extreme P-T conditions are robust with respect to the choice of functional.

We employed a plane-wave basis with ONCV SG15 pseudopotentials [51, 52]. The time step was 0.24 fs. We used deuterium atoms instead of hydrogen atoms in simulations, which allowed for the use of the larger time step. For ease of interpretation of our results, we still refer to these atoms as hydrogen atoms in the text. Temperature in simulations was maintained using the Bussi-Donadio-Parrinello thermostat [53], with a relaxation time of 24.2 fs. We performed constant pressure (NPT) simulations until the unit cell volume converged. In these variable-cell AIMD simulations, the plane-wave energy cutoff was set to 85 Ry, with the reference cell energy cutoff set to 70 Ry [54]. After the unit cell volume converged at the desired P-T conditions, a new unit cell was constructed to start constant volume (NVT) simulations, where the plane-wave energy cutoff was 65 Ry. The cutoff was

increased to 85 Ry to verify the pressure. The pressure in NVT simulations was computed before reactions occurred in the simulation, i.e., for the mixture of reactants. In the supporting information, we show the potential energy as a function of time (Fig. S1–S4). We considered the simulations equilibrated when there were no longer large fluctuations in the total energy. The equilibration time was different for each run, depending on the initial configuration of the system. Table SI in the supporting information summarizes the simulation set-ups.

Structure determination

The atoms in the first peak in the C-C and C-O RDFs form covalent bonds with the reference C atom. Therefore, the first minimum in the RDF, obtained from the production runs of NVT simulations, is used as the cutoff distance for C-C and C-O bonds at each P-T condition. Table SII in the supporting information lists all the cutoff distances. Each hydrogen atom is considered bonded to its nearest neighbor, unless the nearest neighbor is another hydrogen atom bonded to a third atom. In such cases, the hydrogen instead bonds to its second-nearest neighbor. This allows us to determine the atoms and connectivity in each molecule.

Oxidation state

To calculate the oxidation state of carbon atoms, we computed their local charge, defined as the sum of the nuclear charge (+4e for carbon, considering only valence electrons) and the electronic charge associated with each carbon atom, based on the assumption that all oxygen atoms have an oxidation state of -2, and all hydrogen atoms have an oxidation state of +1. The local electronic charge, q_{local} , was obtained by tracking the maximally localized Wannier function (MLWF) centers [55], which each correspond to an electron pair with charge -2e. For each NVT trajectory, we performed an extra 5 ps of simulation in which

we computed the MLWF centers every 10 time steps. The MLWF centers, denoted M, were considered to be localized on their nearest-neighbor atom. MLWF centers were assigned to a carbon-carbon bond between two carbon atoms C¹ and C² if both the M-C¹ and M-C² distances were smaller than the C¹-C² distance, and the C¹-M-C² angle was larger than 111°. The choice of angle was the smallest possible angle that avoided ambiguity in most of the assignments of MLWF centers to C-C bonds. This determined C-C single, double, and triple bonds. The only exception was cyclobutane-1,2,3,4-tetrone (C₄O₄), where MLWF centers sometimes drifted towards the center of the four-membered ring leading to inconclusive assignments. For those molecules, we assigned all carbon-carbon bonds as single bonds. MLWF centers nearest H in C-H bonds were associated to that bond, and MLWF centers nearest the O in C-O-C, C=O, C≡O (carbon monoxide), C-O⁻ and C-OH were associated to that functional group. Unassigned centers nearest to carbon were considered lone pairs, although these were found only transiently in simulations.

The total electronic charge in C-O and C-H bonds, as determined from the MLWF centers, was divided between the carbon atom and the bonded partner in the usual way. For example, in C=O bonds, there are 4 electrons in the bond and two lone pairs on the oxygen atom. Since O has an oxidation state of -2, all electronic charge in the bond is assigned to the oxygen, and none to the carbon atom. Electrons in carbon-carbon bonds were assumed to be shared equally between C atoms. Lone pairs on carbon atoms contributed -2e of negative charge to the local charge of the carbon. Summing these contributions yielded q_{local} for each carbon atom, and the oxidation state was computed as

SUPPORTING INFORMATION

Details of simulations, energy in simulations, covalent bond length cutoff distances, change in the number of bonds per carbon atom, illustrated examples of reaction mechanisms.

ACKNOWLEDGEMENTS

This work was supported by the Hong Kong Research Grants Council (RGC) (Projects GRF-16301723 and GRF-16306621), and National Natural Science Foundation of China/RGC Joint Research Scheme (N_HKUST664/24). Part of this work was carried out using computational resources from the National Supercomputer Center in Guangzhou, China.

* Present address: Lehrstuhl für Theoretische Chemie, Ruhr-Universität Bochum, 44780 Bochum, Germany

† bruceli@ust.hk

‡ dingpan@ust.hk

- [1] Sherwood Lollar, B., Westgate, T. D., Ward, J. A., Slater, G. F. & Lacrampe-Couloume, G. Abiogenic formation of alkanes in the Earth's crust as a minor source for global hydrocarbon reservoirs. *Nature* **416**, 522–524 (2002).
- [2] Sherwood Lollar, B. *et al.* Unravelling abiogenic and biogenic sources of methane in the Earth's deep subsurface. *Chem. Geol.* **226**, 328–339 (2006).
- [3] Proskurowski, G. *et al.* Abiogenic hydrocarbon production at Lost City hydrothermal field. *Science* **319**, 604–607 (2008).
- [4] Cao, M. J., Qin, K. Z., Li, G. M., Evans, N. J. & Jin, L. Y. Abiogenic Fischer-Tropsch synthesis of methane at the Baogutu reduced porphyry copper deposit, western Junggar, NW-China. *Geochim. Cosmochim. Acta* **141**, 179–198 (2014).
- [5] Kelemen, P. B. & Manning, C. E. Reevaluating carbon fluxes in subduction zones, what goes down, mostly comes up. *Proc. Natl. Acad. Sci. U. S. A.* **112**, E3997–E4006 (2015).
- [6] Kutcherov, V. G., Ivanov, K., Mukhina, E. & Serovaiskii, A. Deep hydrocarbon cycle: An experimental simulation. In Manning, C. E., Lin, J.-F. & Mao, W. L. (eds.) *Carbon in Earth's*

Interior, chap. 26, 329–339 (John Wiley & Sons, Inc., 2020), 1 edn.

- [7] Kutcherov, V. G. & Krayushkin, V. A. Deep-seated abiogenic origin of petroleum: From geological assessment to physical theory. *Rev. Geophys.* **48**, RG1001 (2010).
- [8] Mendeleev, D. L'origine du pétrole. *Rev. Sci.* **8**, 409–416 (1877).
- [9] Gold, T. & Soter, S. The deep-Earth-gas hypothesis. *Sci. Am.* **242**, 154–161 (1980).
- [10] Sephton, M. A. & Hazen, R. M. On the origins of deep hydrocarbons. *Rev. Mineral. Geochem.* **75**, 449–465 (2013).
- [11] Beyazay, T. *et al.* Influence of composition of nickel-iron nanoparticles for abiotic CO₂ conversion to early prebiotic organics. *Angew. Chem., Int. Ed.* **135**, e202218189 (2023).
- [12] Brady III, R. C. & Pettit, R. On the mechanism of the Fischer-Tropsch reaction. The chain propagation step. *J. Am. Chem. Soc.* **103**, 1287–1289 (1981).
- [13] McCollom, T. M. Laboratory simulations of abiotic hydrocarbon formation in Earth's deep subsurface. *Rev. Mineral. Geochem.* **75**, 467–494 (2013).
- [14] Thompson, A. B. Water in the Earth's upper mantle. *Nature* **358**, 295–302 (1992).
- [15] Kolesnikov, A., Kutcherov, V. G. & Goncharov, A. F. Methane-derived hydrocarbons produced under upper-mantle conditions. *Nat. Geosci.* **2**, 566–570 (2009).
- [16] Gygi, F. & Galli, G. Ab initio simulation in extreme conditions. *Mater. Today* **8**, 26–32 (2005).
- [17] Spanu, L., Donadio, D., Hohl, D., Schwegler, E. & Galli, G. Stability of hydrocarbons at deep Earth pressures and temperatures. *Proc. Natl. Acad. Sci. U. S. A.* **108**, 6843–6846 (2011).
- [18] Kuang, H. & Tse, J. S. High-Temperature, High-Pressure reactions of H₂ with CaCO₃ melts. *Phys. Status Solidi B* **259**, 2100644 (2022).
- [19] Ancilotto, F., Chiarotti, G. L., Scandolo, S. & Tosatti, E. Dissociation of methane into hydrocarbons at extreme (planetary) pressure and temperature. *Science* **275**, 1288–1290 (1997).

[20] Lee, M.-S. & Scandolo, S. Mixtures of planetary ices at extreme conditions. *Nat. Commun.* **2**, 185 (2011).

[21] Li, D., Zhang, P. & Yan, J. Quantum molecular dynamics simulations for the nonmetal-metal transition in shocked methane. *Phys. Rev. B* **84**, 184204 (2011).

[22] Schröder, D. *et al.* Ethylenedione: An intrinsically short-lived molecule. *Chem. Eur. J.* **4**, 2550–2557 (1998).

[23] Xin, J.-F., Han, X.-R., He, F.-F. & Ding, Y.-H. Global isomeric survey of elusive cyclopropanetrione: Unknown but viable isomers. *Front. Chem.* **7** (2019).

[24] Mato, J., Poole, D. & Gordon, M. S. Stability and dissociation of ethylenedione (OCCO). *J. Phys. Chem. A* **124**, 8209–8222 (2020).

[25] Gleiter, R., Hyla-Kryspin, I. & Pfeifer, K. H. On the stability of the tetramers of carbon monoxide, hydrogen isocyanide, and vinylidene. A molecular orbital theoretical rationalization. *J. Org. Chem.* **60**, 5878–5883 (1995).

[26] Guo, J. C., Hou, G. L., Li, S. D. & Wang, X. B. Probing the low-lying electronic states of cyclobutanetetraone (C_4O_4) and its radical anion: A low-temperature anion photoelectron spectroscopic approach. *J. Phys. Chem. Lett.* **3**, 304–308 (2012).

[27] McCollom, T. M., Ritter, G. & Simoneit, B. R. Lipid synthesis under hydrothermal conditions by Fischer-Tropsch-type reactions. *Origins Life Evol. B.* **29**, 153–166 (1999).

[28] Berndt, M. E., Allen, D. E. & Seyfried Jr, W. E. Reduction of CO_2 during serpentinization of olivine at 300 °C and 500 bar. *Geology* **24**, 351–354 (1996).

[29] McCollom, T. M. & Seewald, J. S. Carbon isotope composition of organic compounds produced by abiotic synthesis under hydrothermal conditions. *Earth Planet. Sci. Lett.* **243**, 74–84 (2006).

[30] Kutcherov, V., Kolesnikov, A., Dyuzheva, T. & Brazhkin, V. Synthesis of hydrocarbons under upper mantle conditions: Evidence for the theory of abiotic deep petroleum origin. In *J. Phys.: Conf. Ser.*, vol. 215, 012103 (IOP Publishing, 2010).

- [31] Belonoshko, A. B., Lukinov, T., Rosengren, A., Bryk, T. & Litasov, K. D. Synthesis of heavy hydrocarbons at the core-mantle boundary. *Sci. Rep.* **5**, 18382 (2015).
- [32] Horita, J. & Berndt, M. E. Abiogenic methane formation and isotopic fractionation under hydrothermal conditions. *Science* **285**, 1055–1057 (1999).
- [33] Sokol, A., Tomilenko, A., Sokol, I., Zaikin, P. & Bul'bak, T. Formation of hydrocarbons in the presence of native iron under upper mantle conditions: Experimental constraints. *Minerals* **10**, 88 (2020).
- [34] Sokol, A. G., Palyanova, G. A., Palyanov, Y. N., Tomilenko, A. A. & Melenovsky, V. N. Fluid regime and diamond formation in the reduced mantle: Experimental constraints. *Geochim. Cosmochim. Acta* **73**, 5820–5834 (2009).
- [35] Sokol, A. G. *et al.* Carbon and Nitrogen Speciation in N-poor COHN Fluids at 6.3 GPa and 1100–1400 °C. *Sci. Rep.* **7**, 706 (2017).
- [36] Foustoukos, D. I. & Seyfried, W. E. Hydrocarbons in hydrothermal vent fluids: The role of chromium-bearing catalysts. *Science* **304**, 1002–1005 (2004).
- [37] Lang, S. Q. *et al.* Microbial utilization of abiogenic carbon and hydrogen in a serpentinite-hosted system. *Geochim. Cosmochim. Acta* **92**, 82–99 (2012).
- [38] McDermott, J. M., Seewald, J. S., German, C. R. & Sylva, S. P. Pathways for abiotic organic synthesis at submarine hydrothermal fields. *Proc. Natl. Acad. Sci. U. S. A.* **112**, 7668–7672 (2015).
- [39] Plank, T. & Manning, C. E. Subducting carbon. *Nature* **574**, 343–352 (2019).
- [40] Huang, F., Daniel, I., Cardon, H., Montagnac, G. & Sverjensky, D. A. Immiscible hydrocarbon fluids in the deep carbon cycle. *Nat. Commun.* **8**, 15798 (2017).
- [41] Mukhina, E., Kolesnikov, A. & Kutcherov, V. The lower pT limit of deep hydrocarbon synthesis by CaCO_3 aqueous reduction. *Sci. Rep.* **7**, 5749 (2017).
- [42] Gygi, F. Architecture of Qbox: A scalable first-principles molecular dynamics code. *IBM J. Res. Dev.* **52**, 137–144 (2008).

[43] Perdew, J. P., Burke, K. & Ernzerhof, M. Generalized gradient approximation made simple. *Phys. Rev. Lett.* **77**, 3865–3868 (1996).

[44] Adamo, C. & Barone, V. Toward reliable density functional methods without adjustable parameters: The PBE0 model. *J. Chem. Phys.* **110**, 6158–6170 (1999).

[45] Pan, D., Spanu, L., Harrison, B., Sverjensky, D. A. & Galli, G. Dielectric properties of water under extreme conditions and transport of carbonates in the deep Earth. *Proc. Natl. Acad. Sci. U. S. A.* **110**, 6646–6650 (2013).

[46] Pan, D., Wan, Q. & Galli, G. The refractive index and electronic gap of water and ice increase with increasing pressure. *Nat. Commun.* **5**, 3919 (2014).

[47] Pan, D. & Galli, G. The fate of carbon dioxide in water-rich fluids under extreme conditions. *Sci. Adv.* **2**, e1601278 (2016).

[48] Grimme, S., Antony, J., Ehrlich, S. & Krieg, H. A consistent and accurate ab initio parametrization of density functional dispersion correction (DFT-D) for the 94 elements H-Pu. *J. Chem. Phys.* **132**, 154104 (2010).

[49] Hammer, B., Hansen, L. B. & Nørskov, J. K. Improved adsorption energetics within density-functional theory using revised Perdew-Burke-Ernzerhof functionals. *Phys. Rev. B* **59**, 7413–7421 (1999).

[50] Stolte, N., Hou, R. & Pan, D. Nanoconfinement facilitates reactions of carbon dioxide in supercritical water. *Nat. Commun.* **13**, 5932 (2022).

[51] Hamann, D. R. Optimized norm-conserving Vanderbilt pseudopotentials. *Phys. Rev. B* **88**, 085117 (2013).

[52] Schlipf, M. & Gygi, F. Optimization algorithm for the generation of ONCV pseudopotentials. *Comput. Phys. Commun.* **196**, 36–44 (2015).

[53] Bussi, G., Donadio, D. & Parrinello, M. Canonical sampling through velocity rescaling. *J. Chem. Phys.* **126**, 014101 (2007).

- [54] Focher, P., Chiarotti, G. L., Bernasconi, M., Tosatti, E. & Parrinello, M. Structural phase transformations via first-principles simulation. *Europhys. Lett.* **26**, 345 (1994).
- [55] Marzari, N., Mostofi, A. A., Yates, J. R., Souza, I. & Vanderbilt, D. Maximally localized Wannier functions: Theory and applications. *Rev. Mod. Phys.* **84**, 1419–1475 (2012).

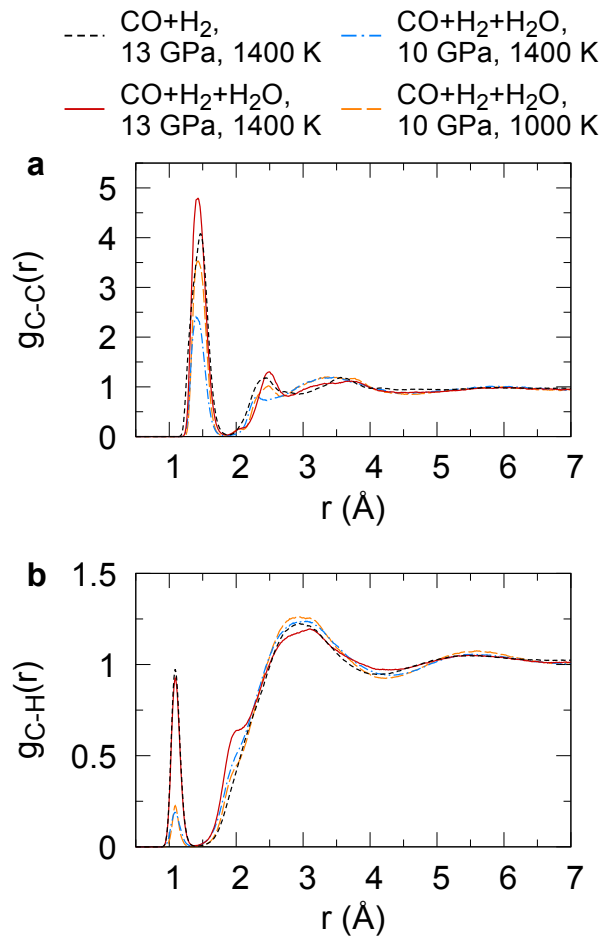


FIG. 1. Carbon-carbon (a) and carbon-hydrogen (b) radial distribution functions for mixtures of CO, H₂ and H₂O.

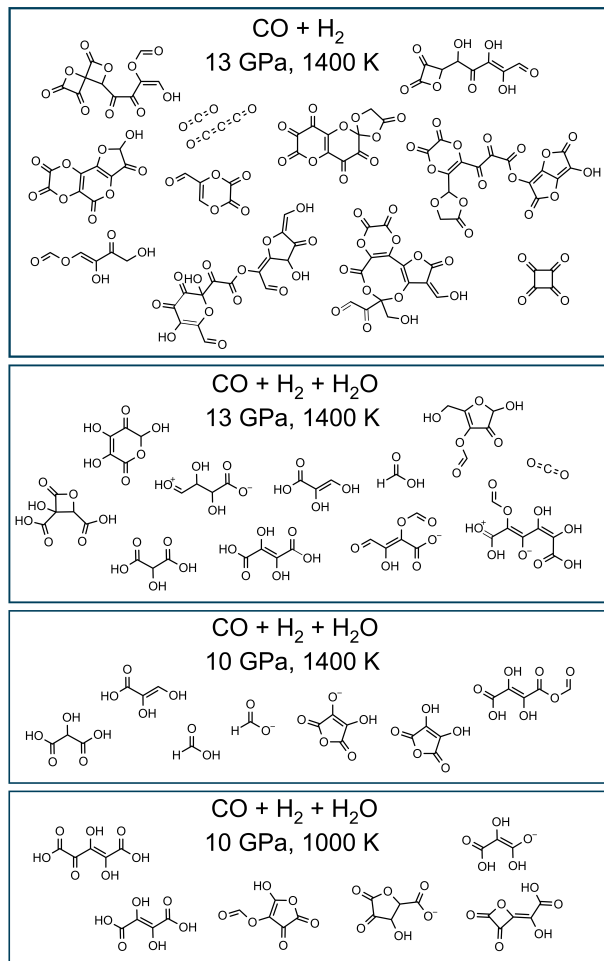


FIG. 2. Reaction products in mixtures of CO, H₂ and H₂O at different P-T conditions. In addition to these products, a substantial amount of CO, H₂, and H₂O remained.

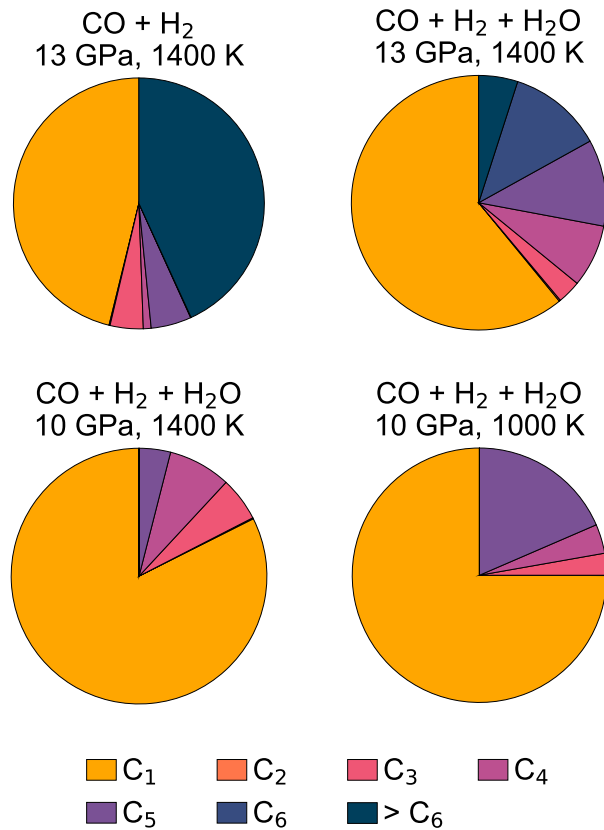


FIG. 3. Fraction of total carbon in C_n molecules produced in mixtures of CO , H_2 and H_2O . n is the number of carbon atoms in the molecule.

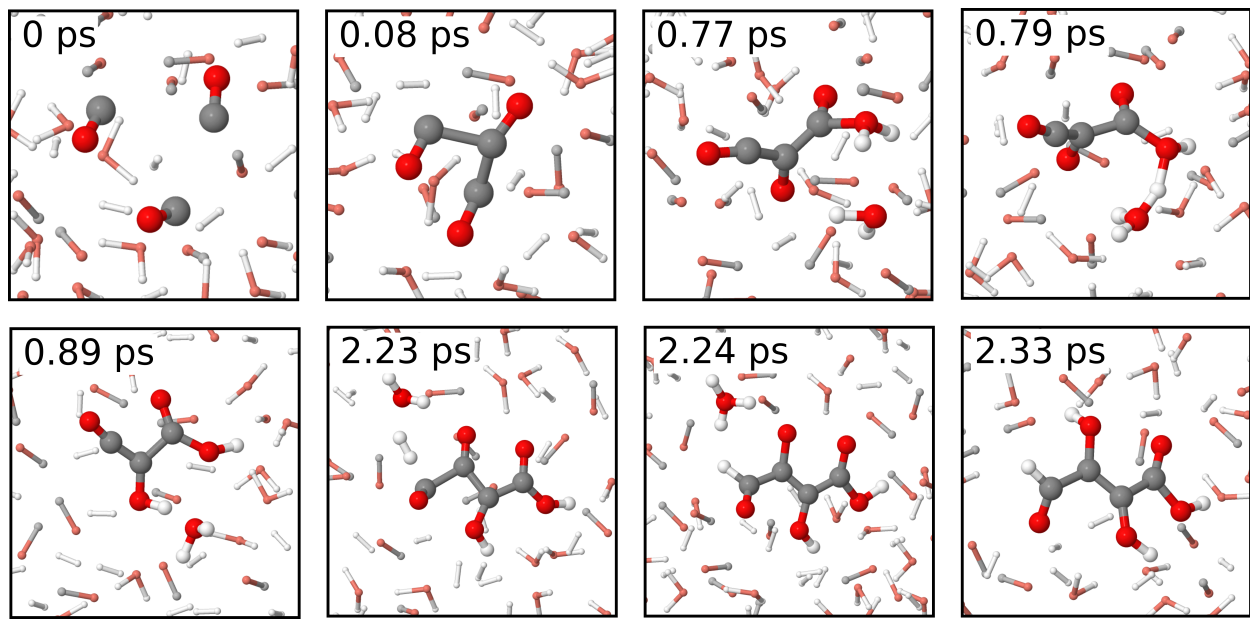


FIG. 4. Formation of 2,3-hydroxy-4-oxobut-2-enoic acid from CO, H₂ and H₂O at 13 GPa and 1400 K.

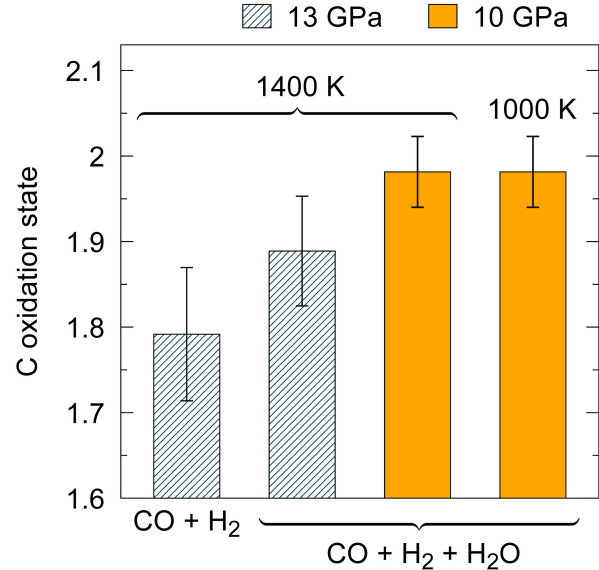


FIG. 5. The mean oxidation state of carbon atoms in the different mixtures of CO, H₂ and H₂O.

The hatched bars show data at 13 GPa, and the solid bars show data at 10 GPa. Temperature is indicated above the bars, and composition is indicated below the bars. The local charge on C atoms and their bonded neighbors was determined using the maximally localized Wannier function centers to localize electrons [55], so that the oxidation state of carbon could be deduced. The error bars show the standard deviation of the mean oxidation state at each time step in simulations.